SEDIMENTOLOGY the journal of the International Association of Sedimentologists

Sedimentology (2023) **70**, 2196–2219 doi: 10.1111/sed.13118

Quantifying the sensitivity of distributive fluvial systems to changes in sediment supply and lake level using stratigraphic forward modelling

SWIAD SNIEDER* , CEDRIC M. GRIFFITHS†,‡, JOHN A. HOWELL*, ADRIAN J. HARTLEY* and AMANDA OWEN§

**School of Geosciences, Meston Building, Kings College, Aberdeen AB24 3UE, UK (E-mail: swiadsnieder@gmail.com)*

†StrataMod Pty Ltd, PO Box 4044, Swan View, WA 6056, Australia

‡Curtin University, Kent Street, Bentley, WA 6102, Australia

§School of Geographical and Earth Sciences, University of Glasgow, Molema Building, University Avenue, Glasgow G12 8QQ, UK

Associate Editor – Christopher Fielding

ABSTRACT

Stratigraphic forward modelling has been used to quantify the sensitivity of sandbody connectivity in a distributive fluvial system to changes in sediment supply and lake level. Recent stratigraphic forward modelling using SedsimX from StrataMod Pty Limited of the Oligocene to Miocene Huesca distributive fluvial system in northern Spain was used as a base-case for this sensitivity analysis. Based on literature research and initial modelling, a sediment supply sensitivity range of 0.22 to 21.85 km^3/kyr and lake-level sensitivity range of −1000 to 1000 mm/kyr were used. Results show that the stratigraphic architecture of the modelled distributive fluvial system is more sensitive to changes in sediment supply than to changes in lake level. While an increase in the rate of sediment supply results in an increase in preserved average grain size, aggradation rates and sandbody connectivity at the same distance from the apex, the average grain size, aggradation rate and sandbody connectivity all decrease with increasing distance from fan apex. The main difference in the stratigraphic architecture can be found in the proximal zones. Only oversupplied models, with much higher sediment supply than the base-case, deposited fully amalgamated channelized deposits with laterally continuous, tabular beds with occasional scoured surfaces. Models with base-case sediment supply contain channelized sandy deposits within a fine-grained floodplain environment. Models with sediment supply much lower than the base-case had no deposition in the proximal zone. Lake-level rise leads to reduced distal erosion of sediments, concentration of silts close to the lake shore, and higher aggradation rates and thicker sandbodies in the proximal zone. The sensitivity analysis highlights that the parameters governing the formation of distributive fluvial systems have different weightings but are ultimately all interconnected and interdependent. This quantitative framework can be used as a predictive tool for subsurface exploration in distributive fluvial systems.

Keywords Distributive fluvial systems, lake-level change, quantitative sedimentology, sediment supply, sensitivity analysis, stratigraphic forward modelling.

INTRODUCTION

A key requirement in the analysis of fluvial systems is understanding the role of allocyclic and autocyclic controls on the subsequent alluvial architecture (Best & Fielding, 2019). To assess the relative importance of these controls it is important to be able to isolate the response of an individual fluvial system to changes in autocyclic or allocyclic drivers. Hydraulic process-based forward modelling provides a mechanism to do this. It allows control of input parameters and sampling of the output at the temporal and spatial resolution of the model throughout a system. Such forward models use physical formulae for fluid flow and sediment erosion, transport and deposition typically with field measurements to constrain input parameters and serve to provide a quantitative prediction of the three-dimensional distribution of sediments over realistic temporal and spatial scales. Snieder *et al.* (2021) showed that the hydrodynamic stratigraphic forward modelling software 'SedsimX' can reproduce the key stratigraphic characteristics of a distributive fluvial system (DFS) terminating in a lake. That model was quality checked against the well-studied outcrops of the Late Oligocene to Early Miocene Huesca DFS, Ebro Basin, northern Spain (Snieder *et al.*, 2021), where the resulting model led to key findings, which expand understanding of the stratigraphic architecture of DFS. For example, reservoir characteristics in radial DFS are dependent on the angle away from the meridian (straight line from the source through the apex to the distal zone of the DFS). The larger the angle, the coarser the average grain size within the proximal zone, with the average grain size in the medial and distal zones being finer. In addition, lateral variability of net to gross, sandbody thickness and number, together with amalgamation ratio, is greatest at the transition between the proximal and medial zone and is still significant in the distal part of the DFS. Stratigraphic forward modelling can therefore enhance our understanding of DFS, potentially leading to reduced risk associated with exploration, production, and storage of fluids in subsurface DFS deposits.

Distributive fluvial systems are defined as fluvial systems, that in planform have a distributive channel pattern downstream of the apex. They occur in every climate, tectonic and basin setting (Hartley *et al.*, 2010; Weissmann *et al.*, 2010). Outcrop and subsurface studies of multiple DFS led Nichols & Fisher (2007) and Owen *et al.* (2015) to a generalized description of DFS facies and stratigraphic architecture. The proximal zone is characterized by amalgamated channel-fill facies with limited preservation of associated fine-grained overbank deposits. This makes the proximal zone a single interconnected sandbody. The medial zone is characterized by sandstone-dominated channel-fill deposits within floodplain deposits consisting mainly of mudrocks and sheet-like bodies of sandstone. In general, the grain size and channel width decrease downstream. Sandbodies may be connected laterally, but vertical connectivity is less common (Nichols & Fisher, 2007). The distal zone is dominated by floodplain facies, with sandbodies mostly deposited as thin sheets with isolated ribbon-shaped channelized elements. In the distal zone, sandbodies connect neither laterally nor vertically (Nichols & Fisher, 2007). To distinguish between the facies and stratigraphic architecture zonation described above and the location within the DFS, proximal, medial and distal zones are used for the former, and proximal, medial and distal regions are used for the latter. Extensive remote sensing studies suggest fluvial systems in modern continental basins are mostly classified as DFS (Weissmann *et al.*, 2015) and as a result their accumulated successions may be prevalent in the rock record. These remote sensing studies have shown that 18% of modern DFS terminate in lakes (Hartley *et al.*, 2010).

The key input parameters used in the forward stratigraphic modelling of DFS systems terminating in lakes are: (i) sediment supply at the upstream end of the system; and (ii) lake-level change at the downstream end. Using the Snieder *et al.* (2021) model of the Huesca system in the Ebro Basin as a base-case, this study aims to investigate the sensitivity of stratal architecture within a DFS to:

- rates of sediment supply ranging from 0.22 to 21.85 km^3/kyr;
- rates of lake level change ranging from −1000 to 1000 mm/kyr;
- the interdependence of these variables.

DATA AND METHODS

Stratigraphic forward modelling software

The stratigraphic forward modelling (SFM) software SedsimX from StrataMod Pty Limited, Swan View, WA, Australia, was used for this

study. It is a hydrodynamic, three-dimensional process-based software, which is fully scalable in time and space. SedsimX is deterministic, which means that the same input parameters always produce the same model output as there is no probabilistic component to the software (Tetzlaff & Harbaugh, 1989; Griffiths *et al.*, 2001; Huang *et al.*, 2016; Snieder *et al.*, 2021).

Hydrodynamics are computed using a digital approximation of the Navier–Stokes equation so that open channel flow is modelled in two horizontal dimensions with a depth-averaged flow velocity. The Navier–Stokes equations are a set of partial differential equations (PDEs) in which mathematical objects called operators act on parameters of the flow. The dominant method of calculating fluid flow involves dividing the flow region into thousands or even millions of smaller volumes known as a mesh. In this 'finite-volume' approach, the Navier–Stokes equations are then used to construct equations which can be used to calculate the movement of fluid properties between cells. By repeatedly solving these transport equations over small time periods, a numerical approximation to the behaviour of the flow can be achieved.

The friction parameter (Manning Coefficient) at the water–channel interface is selected to create a realistic depth-velocity profile. Fluid elements (fixed volumes of water representing continuous flow) are released at the source at each time step. The fluid elements then follow the steepest gradient between nodes (cells have nodes at each corner) of the underlying surface at that time step. SedsimX uses a grid of square cells where the number of grid cells (x, y) and the spatial values assigned to each cell (metres) defines the total physical size represented by the simulation grid.

Sediment erosion, transport and deposition is computed in three dimensions using a mixed Lagrangian/Eulerian computational scheme for each node and time step. Mass conservation is maintained (Tetzlaff & Harbaugh, 1989). The critical shear stress determines the boundary between erosion and transportation, calculated as a function of particle diameter and density (Griffiths *et al.*, 2001). The software models each grain as a perfect sphere with a given grain diameter and density. At each display interval, the model outputs relating to sediment thickness and grain-size distribution are stored for each node (Tetzlaff & Harbaugh, 1989). A detailed description of the modelling software SedsimX is given in Snieder *et al.* (2021). SedsimX has been applied to reproduce the stratigraphic architecture of the Late Oligocene to Early Miocene Huesca DFS, Ebro Basin, northern Spain, at true temporal and spatial scales (Snieder *et al.*, 2021).

Units

For discharge, flow velocity and sediment concentrations, SI units of metre (m), second (s) and kilograms (kg) were used. For the sediment supply rate, the unit cubic kilometres per 1000 years (km^3/kyr) was used to create values that are easier to understand. For conversion to SI unit: 1 km^3/kyr = 0.032 m^3/s. For the lake-level change rate, the unit millimetre per 1000 years (mm/kyr) was used to create values that are easier to understand. For conversion to SI unit: 1 mm/kyr = 3.169×10^{-14} m/s.

Sensitivity analysis input parameters

During the modelled duration, sediment supply is defined as the total sediment volume flowing into the model at source (Fig. 1), and lake-level change was modelled as a change in base-level with the starting base-level set to the lowest elevation of the initial surface (Fig. 1). The sensitivity analysis is centred around a base-case model (2.2 km^3/kyr sediment supply and 100 mm/kyr lake-level rise). The Huesca DFS model (Snieder *et al.*, 2021) was used as the base-case model with modified: (i) model duration, time step and display interval; (ii) grid dimensions and initial surface; (iii) sediments; (iv) sources; and (v) lake-level change rate (Table 1).

1 The model duration was 100 kyr, beginning at −100 kyr and ending at 0 kyr, as it allows a display interval of 100 years while keeping the model output file sizes within the limit of the post-processing software. The time step was lowered from five years to one year to give a higher temporal resolution than the Huesca DFS model, and the display interval was lowered from 250 to 100 years (cf. Snieder *et al.*, 2021). The sampling intervals of all SedsimX modules were also changed to match the time step of one year.

2 The model dimensions were enlarged from the base-case model (90 km × 160 km) to 140 km in a north–south direction and 230 km in an east–west direction to enable incorporation and modelling of additional sediments deposited in the high sediment supply models. The initial

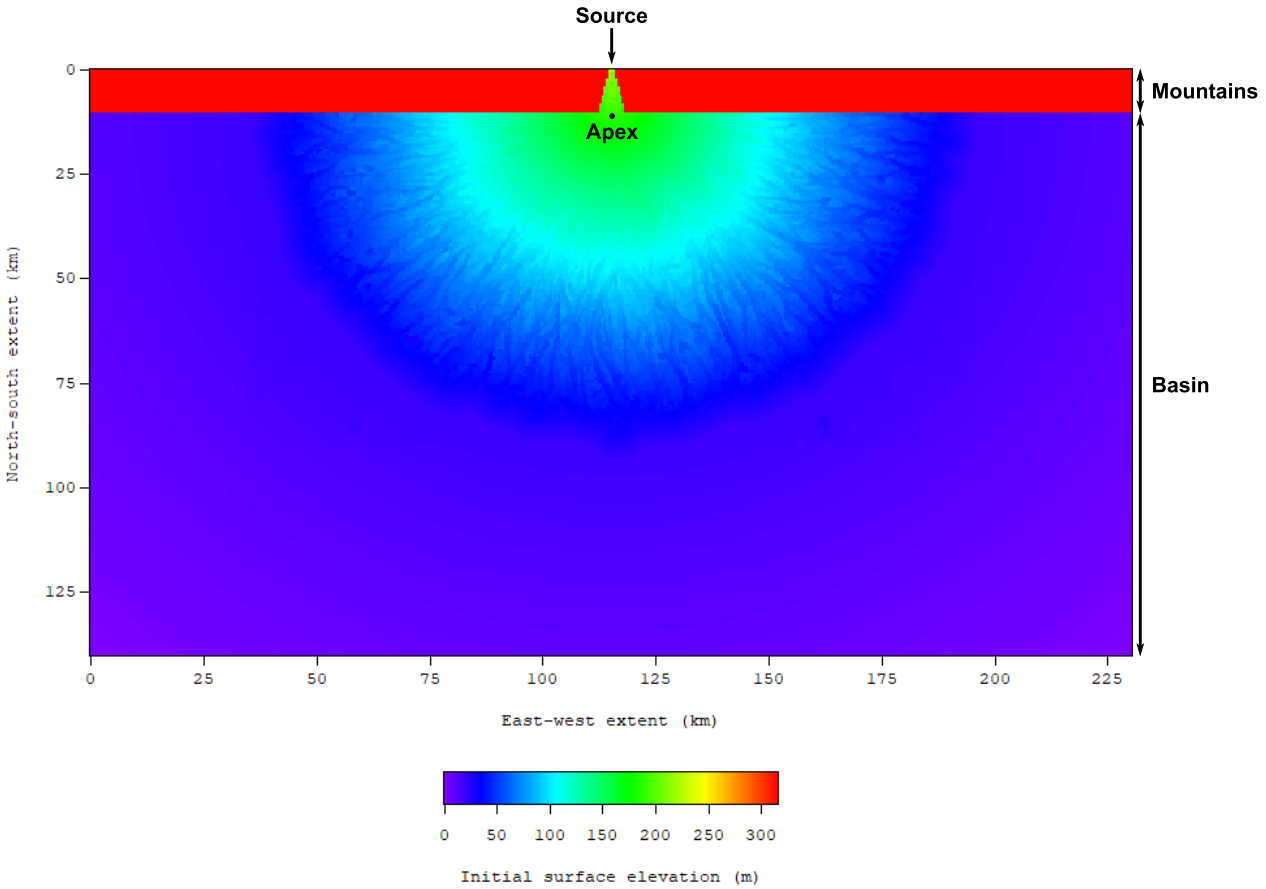

Fig. 1. Initial surface for every model in the sensitivity analysis. It extends 140 km in a north–south direction and 230 km in an east–west direction. It used the depositional surface of the base model at the modelled duration of 125 kyr (Snieder *et al.*, 2021) and extended this depositional surface by 50 km to the south and 35 km to the east and west, respectively, at a gradient of 0.0002 gradient dipping away from the apex.

Table 1. Model input parameters for the sensitivity analysis.

Modules	Description	
Time	Model duration (kyr): 100 Display interval (years): 100 Time step (years): 1	
Grid	Dimensions (km): 140 north–south by 230 east–west Grid size (km): 0.5 × 0.5 Initial surface: See Fig. 1	
Sources	Sampling interval (years): 50 Discharge (Q): See Fig. 2A for base model and appendix for other models Flow velocity (m/s): $0.005 \times Q^{0.825}$ Suspended sediment concentration (kg/m^3): $1.64 \times 10^{-7} \times Q^{2.464}$	
Sediments	Grain sizes (mm) Coarse to medium sands (0.5) Fine to very fine sands (0.125) Silts (0.016) Clays (0.002)	Distribution (%) 0–8 1–13 8–10 71–89
Lake level change rate	Sensitivity analysis steps: −1000, −100, 0, 100 and 1000 mm/kyr	

surface of the model used the depositional surface of the Huesca DFS model at the modelled duration of 125 kyr (Snieder *et al.*, 2021) and extended this depositional surface by 50 km to the south and 35 km to the east and west, respectively. The surface represented by these extensions was assigned an initial gradient of 0.0002, in a direction dipping away from the apex (Fig. 1).

3 The four clastic grain sizes modelled were coarse to medium sand (0.5 mm), fine to very fine sand (0.125 mm), silt (0.016 mm) and clay (0.002 mm). The initial transport type was set to suspended load for all grain sizes, although bed transport would also automatically be modelled if the appropriate hydraulic and load conditions were met. The grain sizes and transport type were derived from the Minnesota River at Fort Snelling State Park, Minnesota, USA (Groten *et al.*, 2016). This hydrological analogue was selected as it spans the range of hydrological parameters used in the sensitivity analysis and is in the same climate zone as the base-case model. The grain-size distribution from the Huesca DFS was not used as the outcrop coverage is not spread over the entire system and can thus not be used as a quantification of the grain-size distribution at system scale. As the hydrological analogue from the Minnesota River provides the grain-size distribution at the source, this was deemed more realistic than an estimate of grain-size distribution from a selection of outcrops (Snieder *et al.*, 2021).

4 The Huesca DFS model used a random distribution of flood events measured from High Island Creek, Minnesota, USA (Groten *et al.*, 2016; Snieder *et al.*, 2021). This hydrological analogue was used because it spans the range of grain sizes found in the Huesca DFS outcrops and its watershed is located in the same climate zone as that interpreted for the Huesca DFS in the Miocene and Pliocene (Snieder *et al.*, 2021). To introduce a link between climate variation and the source parameters for the sensitivity analysis, the source parameters were modulated by a climate proxy curve. This proxy curve is a combination of the low frequency Holocene eustatic sea-level curve derived from oxygen isotope data (Lisiecki & Raymo, 2005) and the high-frequency insolation curve (based on Milankovitch cyclicity) derived from ocean core data (Laskar *et al.*, 2004). It was assumed that the slope of this modulated curve is a proxy for the changes in hinterland erosion, transport and sediment deposition through the medium of rainfall. It was further assumed that source parameters are a function of the rate of change of this curve rather than its absolute value. This means that high rates of increase in insolation are linked to warmer and wetter climates, which lead to increased rates of rainfall, weathering and sediment supply to the basin. Likewise, high rates of falling insolation are linked to cooler and drier conditions, which lead to reduced rates of rainfall, weathering and sediment supply to the basin (Imbrie *et al.*, 1992; Couchoud *et al.*, 2009).

For the sensitivity analysis, the time interval between 0 kyr and 100 kyr before present was chosen as it is covered by sea-level and insolation curves. The climate proxy curve was sampled every 50 years as this allows a 100 year temporal resolution (Nyquist, 1928; Shannon, 1949), which equals the display interval. The hydrological parameters (discharge, flow velocity, sediment concentration and grain-size distribution) were taken from the Minnesota River at Fort Snelling State Park, Minnesota, USA (Groten *et al.*, 2016), as this river spans the range of parameters used in the sensitivity analysis and is in the same climate zone as the base-case model (Snieder *et al.*, 2021). The discharge was driven by the climate proxy for each 50-year sampling step (Figs 2A, S3A, S4A, S5A and S6A) and rating curves (Table 1; Figs S1 and S2) were used to calculate the flow velocity (Figs 2B, S3B, S4B, S5B and S6B) and suspended sediment concentration (Figs 2C, S3C, S4C, S5C and S6C) for each sampling step. This results in time-dependent discharge and flow velocity curves for each model. Because there was no link between discharge and grain-size distribution in the river data, it was randomized within the measured ranges (Table 1; Figs 2D, S3D, S4D, S5D and S6D). Details of the relationship between the climate proxy curve and the source parameters are provided in Appendix S1.

5 The lake-level change occurred at the rate set in the sensitivity analysis matrix (Fig. 3) and all models start at the same lake-level elevation of 0 m (lowest point of the initial surface; Fig. 1). The lake-level rise is not linked to the climate proxy curve described above as this would result in an interdependency of the two sensitivity parameters, sediment supply and lake level. The lake-level in the model is tracked both in elevation and time.

The sensitivity analysis spans two orders of magnitude of sediment supply and four orders of magnitude of lake-level change. This parameter

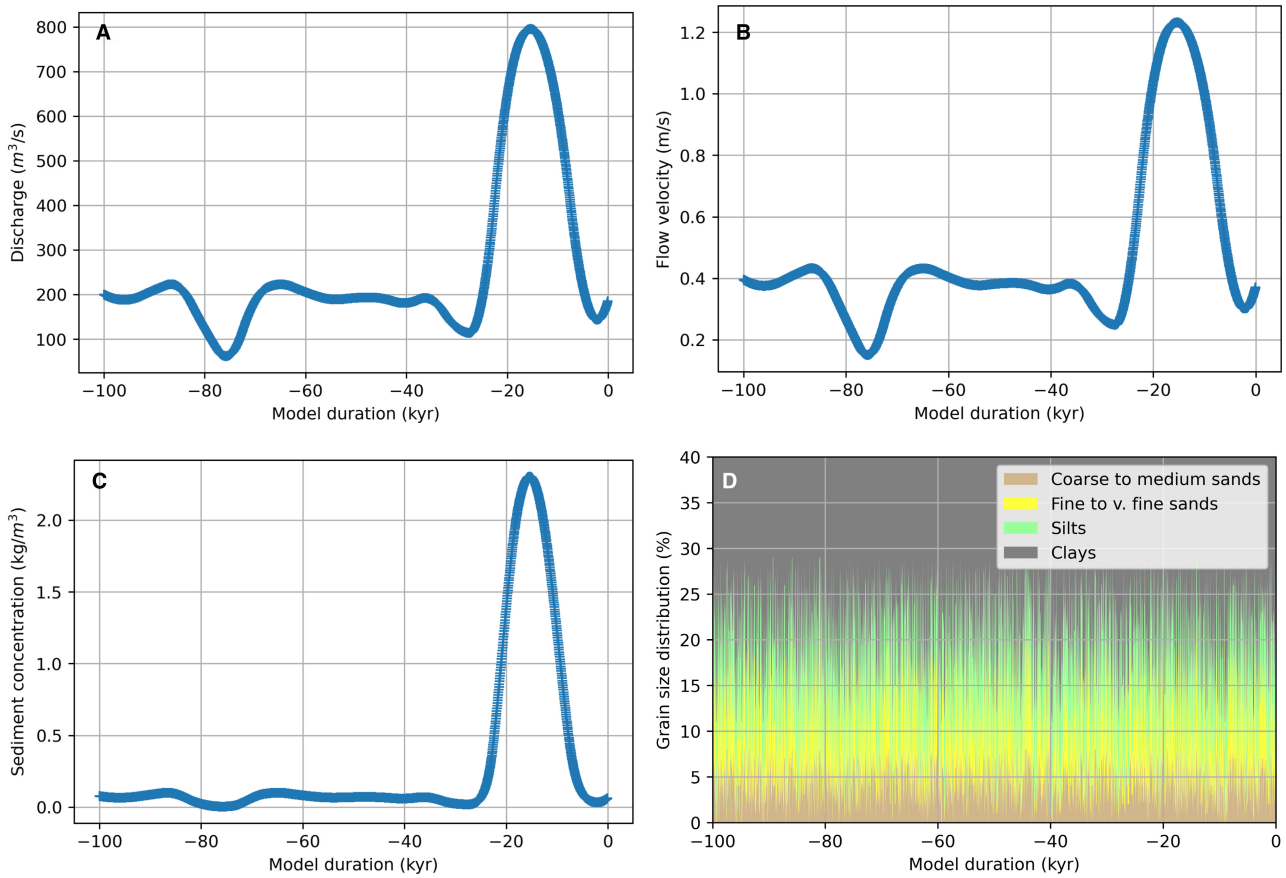

Fig. 2. Hydrological parameters of the medium sediment supply models (2.2 km^3/kyr) at the source: (A) discharge; (B) flow velocity; (C) sediment concentration; and (D) grain-size distribution with 40 to 100% of the distribution made up of clays. The parameters were sampled every 50 years.

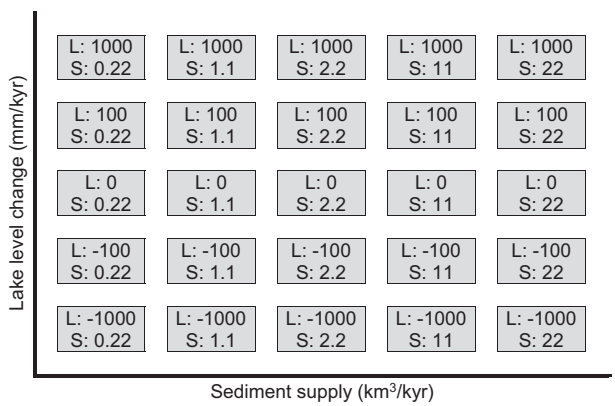

Fig. 3. Sensitivity analysis parameter space of sediment supply (S) and lake level change (L).

space encompasses 25 models (Figs 3 and 4) with five sediment supply columns (0.22, 1.1, 2.2, 11 and 22 km^3/kyr) and five lake-level change rows (−1000, −100, 0, 100 and 1000 mm/kyr). The range of sediment supply was derived from a literature study of fluvial systems by Colombera *et al.* (2015), which found a range of accumulation rates spanning two orders of magnitude (9 to 920 mm/kyr). During its aggradational phase, the Huesca DFS model (base model) had an average accumulation rate of 259 mm/kyr (Snieder *et al.*, 2021), which is approximately one order of magnitude from the minimum and one order of magnitude from the maximum accumulation rate found in the literature study. In order to match the preserved, decompacted volume of the Huesca DFS, and given the 60% compaction and 20% sediment bypass in the model, the necessary sediment supply to the Huesca DFS model was 2.2 km^3/kyr. Because the sediment supply is proportional to the accumulation rate, sediment supply rates ranging an order of magnitude on either side of the Huesca DFS/base-case model were used for the sensitivity analysis. Lake level change rates range from a drop of 1000 mm/kyr to a rise of 1000 mm/kyr as

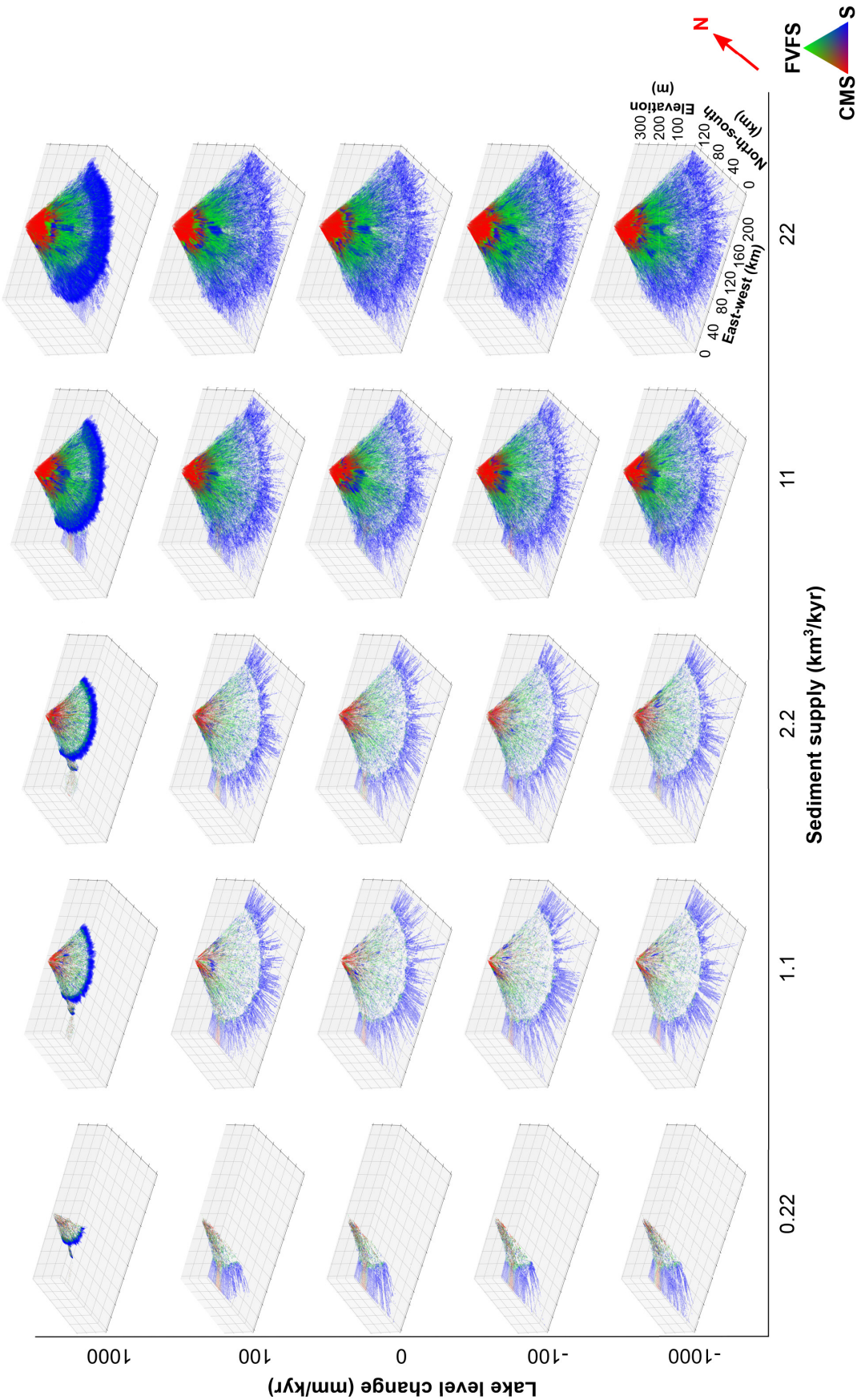

Fig. 4. Sediment supply – lake level change sensitivity models showing grain-size distribution as a point cloud (CMS – coarse to medium sands; FVFS – fine to very fine sands; S – silts). The model axes are scaled and annotated in the bottom left model.

preliminary modelling showed a low impact of lake-level change on the model output. The lake-level change values are all relative to the initial surface. This means that the lake level only rises above the initial surface for the models with a lake-level rise (100 mm/kyr and 1000 mm/kyr). For the lowering and static lake-level change models (−1000 mm/kyr, −100 mm/kyr and 0 mm/kyr, respectively), the lake level drops or stays below the initial surface. The physical formulae for fluid flow and sediment erosion, transport and deposition employed by the stratigraphic forward modelling software use the lake level as base-level. This means that each model has a graded profile approaching the lake level as its lowest erosional envelope. Lowering the lake level increases the differential between the depositional surface and the lowest erosional envelope at any given time. This means that even though the lake level is always below the initial surface for the models with lowering and static lake levels (−1000 mm/kyr, −100 mm/kyr and 0 mm/kyr, respectively), the change still has an influence on the modelled sediment erosion, transport and deposition.

Sensitivity analysis output, data analysis and visualization

The modelling software saves sediment thickness and grain-size distribution for each node at each display interval. This results in a spatial resolution of 1 km by 1 km, which is twice the grid size due to spatial aliasing (Nyquist, 1928; Shannon, 1949) and a 100 year temporal resolution. As stratigraphic architecture is the focus of this study, small-scale stratal units were defined as having a thickness of at least 10 mm (Bridge, 2003). To resolve this minimum thickness, the thinnest layer in the model needs to be no thicker than half the bedding thickness (Nyquist, 1928; Shannon, 1949). The minimum bed thickness at each grid node for every time step is thus 5 mm. To speed up post-processing, all layers with thicknesses <5 mm have been filtered out. Additionally, as the DFS is exclusively deposited south of the apex, all of the model region north of the apex, including the mountains and the feeder channel (Fig. 1), has been excluded from the data analysis.

After filtering the model outputs, grain-size distribution, sediment thickness, net to gross (NTG), sandbody thickness, number of sandbodies and amalgamation ratio were extracted or calculated. Net to gross is the proportion of the rock volume to potentially act as reservoir (Ringrose & Bentley, 2015). For this analysis, 'net' is defined as pre-compaction coarse to medium sand, fine to very fine sand, and silt. Gross encompasses all grain sizes. The default SedsimX porosity–grain-size-distribution–pressure relationship was used for these models, which means that for a coarse to fine ratio >80% the preserved porosity at 2000 m burial is >15%.

Sandbodies are considered to be accumulated and preserved elements of channels or splays, which contain net grain sizes. Amalgamation ratio quantifies vertical connectivity (the higher the ratio, the better the connectivity) and is defined as the fraction of net to net contacts relative to all bed/cell contacts (net to net, net to mud and mud to mud) in a vertical pseudo-well (Zhang *et al.*, 2017).

To visualize the three-dimensional model output in a two-dimensional plot, a pseudo section from the apex to the most distal parts of the model, was chosen. The Euclidian distance between each node and the apex was calculated and all nodes with the same distance from the apex were combined to one point along a proximal to distal section. The equidistant nodes were grouped in 1 km by 1 km bins as this equals the spatial resolution of the model. This visualization approach only works if the DFS is radially biased (i.e. the deposits have similar grain-size distributions downstream of the apex, independent of the angle of the downstream section from the meridian, which is the straight line from the source through the apex to the distal zone of the DFS). The Hurst exponent (Hurst, 1951) was used to test this bias. The exponent has been proven to quantify the clustering of low and high values in vertical stratigraphic sections (Chen & Hiscott, 1999; Mukhopadhyay *et al.*, 2003; Felletti, 2004; Felletti & Bersezio, 2010; Coronel *et al.*, 2020) and is applied to spatial clustering for this study. A Hurst exponent of 0.5 indicates a random distribution and the closer the exponent is to either zero or one, the more clustered the distribution. The exponent was calculated from the four grain-size distributions, sediment thickness and NTG datasets sorted radially, column by column (each south to north transect from west to east), row by row (each west to east transect from south to north) and randomly (test of Hurst exponent). The most clustered distribution was achieved from the radially sorted dataset with the apex at the focal point, followed by column by column and row by row sorted datasets with

Hurst exponents no less than 0.1 smaller. This means that the grain-size distributions, sediment thickness and NTG datasets are radially biased. The randomly sorted datasets generated exponents around 0.5, providing a quality check of the calculation. The radial characteristics of modelled DFS were investigated at greater detail in Snieder *et al.* (2021), which showed that the greater the angle from the north–south median, the coarser the average grain size in the proximal zone but the finer the average grain size in the medial and distal zones.

In the low sediment supply models in particular, a large part of the model area was not covered by sediment at the end of the model run. The data analysis of these low-deposition models resulted in many outliers, which obscured the actual trends seen in three dimensions. Therefore, only distances from the apex with at least 50% coverage (number of cells with deposits larger than the minimum thickness of 5 mm and the same distance from the apex) were plotted. This resulted in blank sections of the plots, especially in the first (0.22 km^3/kyr) sediment supply column. In the NTG and sediment thickness plots, each node is plotted, but the means and modes are only plotted if the 50% coverage rule is met. The detailed description of model limitations and model output analysis and visualization can be found in Snieder *et al.* (2021).

RESULTS

Mass balance

Mass balance (Table 2) documents the sediment input at the source, the deposition of sediments within the model area, and the outflow of sediments through the open model boundaries to the east, south and west (Fig. 1) for the model duration of 100 kyr. The ratio between sediment input and deposition is called sediment retention. There was no consistent pattern linking sediment supply and sediment retention. For all sediment

Table 2. Mass balance for each sensitivity analysis model. Retention (Ret.) indicates the ratio of deposits to input of total sediments in column four and by grain size (CMS – coarse to medium sands, FVFS – fine to very fine sands, silts and clays) in columns five to eight. The colour coding shows high percentages in red and low ones in blue for column four separately, and columns five to eight together.

Lake level change (mm/kyr)	Sediment supply (km^3/kyr)	Deposits (km^3/kyr)	Ret. (%)	CMS: Ret. (%)	FVFS: Ret. (%)	Silts: Ret. (%)	Clays: Ret. (%)
−1000	0.22	0.12	54.9	90.6	88.0	84.0	47.0
−100	0.22	0.12	54.8	90.4	88.0	82.7	47.2
0	0.22	0.12	55.4	90.3	87.6	83.3	47.9
100	0.22	0.13	58.7	90.5	88.0	83.8	51.9
1000	0.22	0.17	77.5	98.7	98.4	97.8	72.4
−1000	1.10	0.64	58.8	91.6	90.1	87.9	51.3
−100	1.10	0.63	57.5	90.8	88.9	86.0	50.0
0	1.10	0.62	57.0	90.3	88.5	85.5	49.5
100	1.10	0.68	62.3	90.6	88.8	86.2	55.9
1000	1.10	0.79	72.5	93.7	91.9	88.9	67.9
−1000	2.18	1.25	57.2	88.2	85.3	81.8	50.5
−100	2.18	1.23	56.4	88.0	85.1	81.5	49.6
0	2.18	1.23	56.3	88.0	85.1	81.4	49.5
100	2.18	1.31	60.2	88.2	85.2	81.5	54.3
1000	2.18	1.50	69.0	92.7	89.6	85.4	64.2
−1000	10.87	6.14	56.5	91.5	86.6	79.6	49.7
−100	10.87	6.18	56.9	91.8	87.2	80.4	50.0
0	10.87	6.14	56.5	91.3	86.4	79.8	49.6
100	10.87	6.34	58.3	91.3	86.7	80.0	51.8
1000	10.87	6.60	60.7	91.6	86.7	79.6	54.8
−1000	21.85	12.19	55.8	93.3	86.3	77.7	48.9
−100	21.85	12.00	54.9	93.0	85.6	77.0	48.0
0	21.85	12.09	55.3	92.5	85.7	77.0	48.5
100	21.85	12.41	56.8	93.6	86.6	77.7	50.1
1000	21.85	13.16	60.2	93.3	86.4	79.2	54.2

supply models with a lake-level change of −1000, −100, 0 and 100 mm/kyr, the difference between the lowest sediment retention and highest sediment retention for each lake-level change scenario was small at 3.9% for −1000 mm/kyr, 2.7% for −100 mm/kyr, 1.7% for 0 mm/kyr and 5.5% for 100 mm/kyr. In these four lake-level change scenarios, the sediment retention was generally lowest in the models with the lowest and highest sediment supply (0.22 km^3/kyr and 21.85 km^3/kyr, respectively) and highest in the second to lowest sediment supply (1.1 km^3/kyr). The sediment supply models with a lake-level change of 1000 mm/kyr had a difference between lowest and highest sediment retention of 17.3% and highest sediment supply model (21.85 km^3/kyr) and the highest retention was linked to the lowest sediment supply model (0.22 km^3/kyr). Lake-level change showed a consistent pattern regarding sediment retention. The models with lake-level changes of −1000, −100 and 0 mm/kyr always had the lowest sediment retention among them and showed <2% variability within their respective sediment supply scenarios. The models with lake-level change of 1000 mm/kyr always had the highest sediment retention. The sediment retention variability within each sediment supply scenario generally decreased with sediment supply from 22.7% for all models with 0.22 km^3/kyr sediment supply, to 15.5% for 1.1 km^3/kyr, to 12.7% for 2.18 km^3/kyr, to 4.2% for 10.87 km^3/kyr, and finally rose slightly again to 4.9% for 21.85 km^3/kyr.

Sediment retention also decreased with decreasing grain size (Table 2). Sediment retention was higher for coarse to medium sands (ranges 88.0 to 98.7%), fine to very fine sands (ranges 85.1 to 98.4%) and silts (ranges 77 to 97.8%) than for clays (ranges 47 to 72.4%). Variability within each grain size sediment retention group also decreased with grain size: 10.7% for coarse to medium sands, 13.3% for fine to very fine sands, 20.8% for silts and 25.4% for clays. The highest impact on overall sediment retention came from the clay grain size, which comprised 71 to 89% of the sediment input (Table 1).

Three-dimensional and cross-sectional view of models

The three-dimensional images (Fig. 4) show the distribution of the three net grain sizes (coarse to medium sands in red, fine to very fine sands in green, and silts in blue). In general, the models were more sensitive to sediment supply change than to lake-level change. The higher the sediment supply, the greater the sediment volume deposited during the 100 kyr model duration. Deposition in all models started in the south-western sector (Fig. 4). In all but the highest sediment supply models (22 km^3/kyr) coarse to medium sand and fine to very fine sand bypassed the proximal and medial zones to be deposited in the distal zones. Most sedimentation only started when the hydrological parameter discharge exceeded approximately 300 m^3/s for the first time. The greater the sediment input to the models, the earlier during the model duration that depositional threshold was exceeded. The lowest sediment supply models (0.22 km^3/kyr) only reached that threshold at −22 kyr, the second lowest ones (1.1 km^3/kyr) at −24 kyr, the middle ones (2.2 km^3/kyr) at −25 kyr, the two highest sediment supply models (11 km^3/kyr and 22 km^3/kyr, respectively) started above the threshold. When the discharge dropped below the threshold again at a later stage in the modelling process, deposition continued, albeit at a reduced rate. This reduced rate of deposition was still higher at the same discharge than before the threshold was reached. For the models in the lowest sediment supply column (0.22 km^3/kyr), sediments were only deposited in the south-western section whereas the models with higher sediment supply (1.1 to 22 km^3/kyr) blanketed most of the initial surface above the lake level. Additionally, the higher the sediment supply, the clearer the zonation into: (i) homolithic proximal zones of coarse to medium sands; (ii) heterolithic medial zones with a mixture of fine to very fine sand and silt; and (iii) heterolithic distal deposits with silts and clays. The distance from the apex of the transitions between these zones changed with time. The higher the hydrological parameters, the further away from the apex the transitions between zones were located. As the hydrological parameters decreased towards the end of the model duration (Fig. 4), the proximal, medial and distal zones were deposited on top of the proximal zone deposited during the hydrological parameter spike around −17 kyr. This is especially clear in the model with a sediment supply of 22 km^3/kyr and a lake-level change of 1000 mm/kyr (Fig. 4) where all three net grain sizes were deposited in the previously proximal zone with clear transitions between grain sizes and a decrease in grain size downstream of the apex. The models experiencing a static or falling lake level (−1000, −100 and 0 mm/kyr) are very

similar in their three-dimensional net grain-size distribution. Models with rising lake level (100 and 1000 mm/kyr) show that the rising lake concentrated the sediments closer to the apex, having the greatest impact on the silt and clay grain sizes (Fig. 4 and Table 2).

Cross-sections from the apex to the south (Fig. 5) and from the west to the apex (Fig. 6) show the vertical change in the stratigraphic architecture of the models. Figure 5 shows the middle and highest sediment supply models (2.2 and 22 km^3/kyr, respectively) as there was no deposition from the apex to the south in the lowest sediment supply models (0.22 km^3/kyr; Fig. 4). These cross-sections show that three-dimensional sandbody connectivity is more sensitive to sediment supply than to lake-level change. No deposition occurred close to the apex in the lowest sediment supply models (0.22 km^3/kyr) and further downstream channelized sands, enclosed within a floodplain environment, transitioned to a clay dominated distal zone (Fig. 6). The middle sediment supply models (2.2 km^3/kyr) showed the sandy channel elements with lateral splay elements cutting into underlying floodplain deposits from the apex to the distal zone, which was again dominated by clay (Figs 5 and 6). The highest sediment supply models (22 km^3kyr) had a fully amalgamated proximal zone mostly containing sands and a medial zone characterized by sandy channel belt deposits enclosed within overbank mudstones with increasing clay percentage downstream of the apex until it transitioned to the clay dominated distal zone (Figs 5 and 6). As might be anticipated, lake-level change influenced the stratigraphic architecture of the deposits. Sediment was deposited further from the apex in the models with static and lowering lake level than in the models with lake-level rise (Fig. 4). Additionally, static and lowering lake level led to a more progradational stacking pattern while lake-level rise

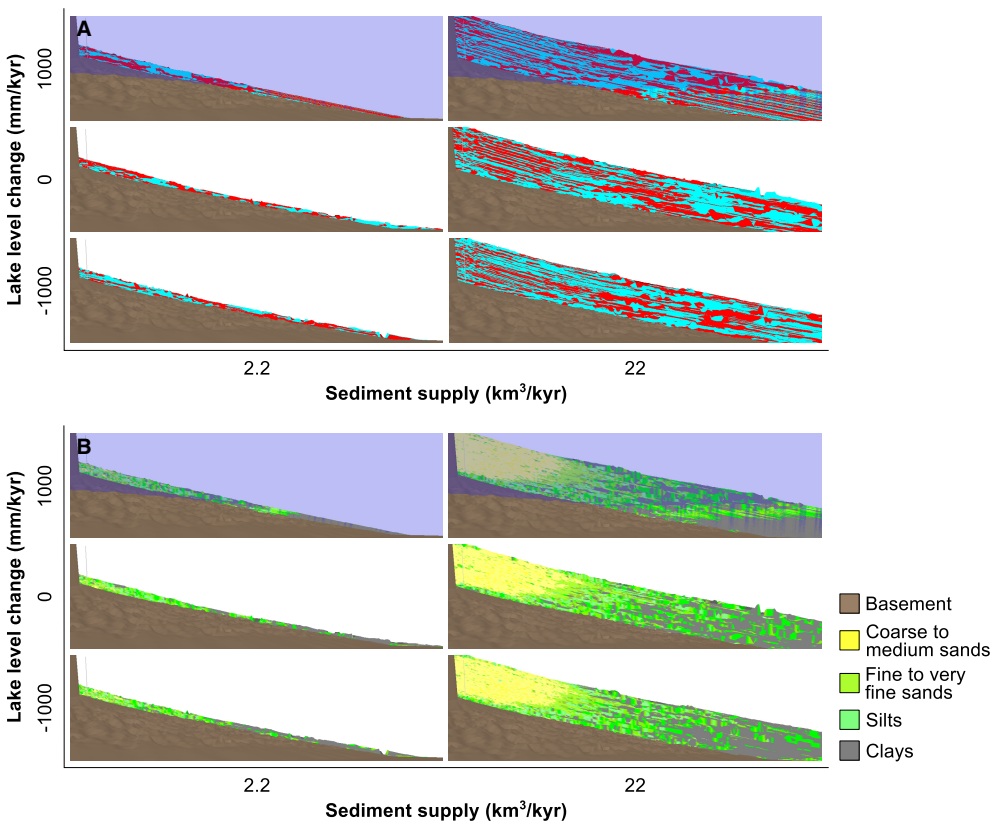

Fig. 5. Sediment supply – lake level change sensitivity models showing: (A) layering (changing colour between red and blue for each alternate display interval); and (B) grain-size distribution. The cross-sections are oriented from the apex on the left towards the south to the right. Only two sediment supply columns and three lake level change rows are shown to preserve the details of each cross-section. The lowest sediment supply column (0.22 km^3/kyr) did not have any deposits along this section. In light blue the lake level at the end of the model duration is shown.

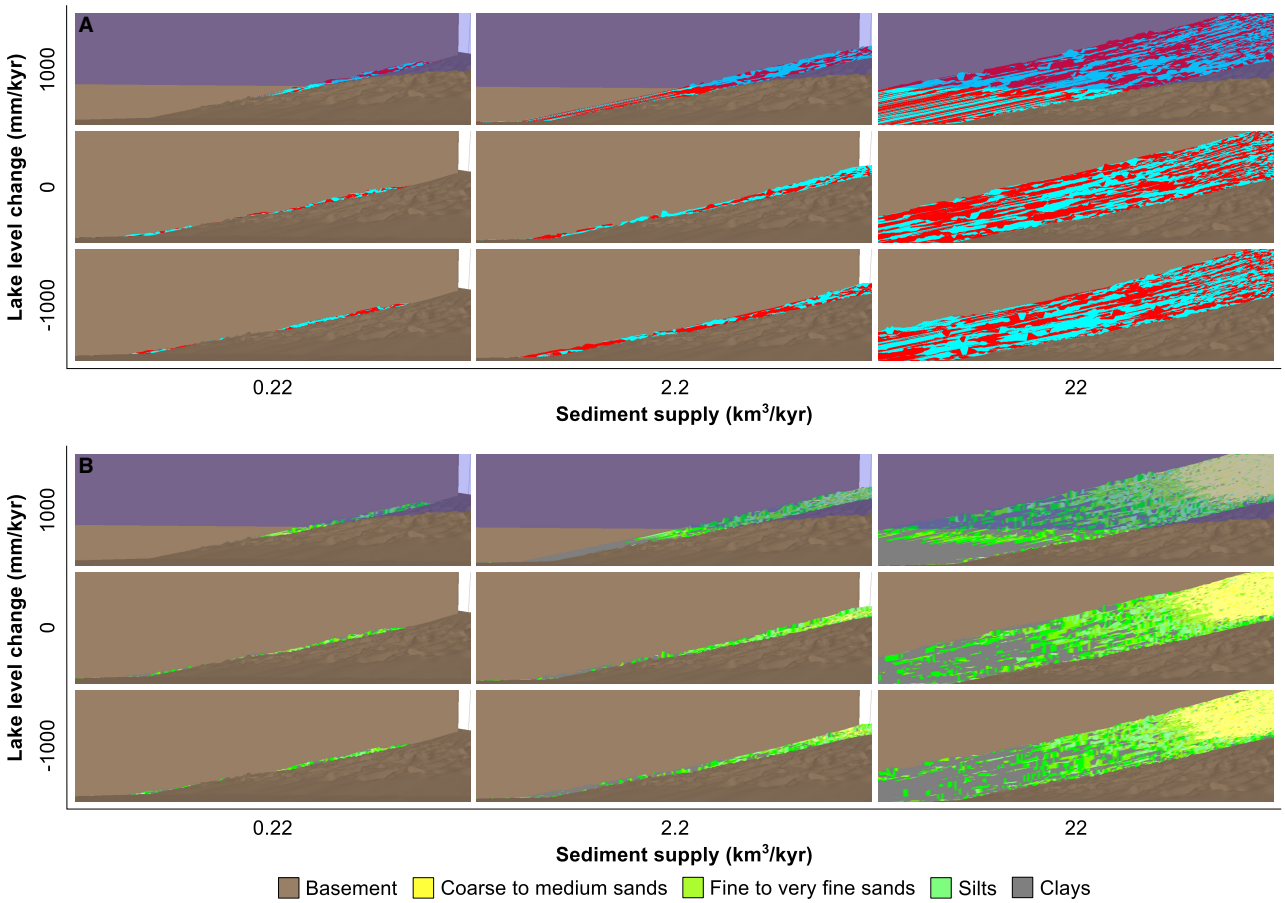

Fig. 6. Sediment supply – lake level change sensitivity models showing: (A) layering (changing colour between red and blue for each alternate display interval); and (B) grain-size distribution. The cross-sections are oriented from the western part of the model on the left to the apex on the right. Only three sediment supply columns and three lake level change rows are shown to preserve the details of each cross-section. In light blue the lake level at the end of the model duration is shown.

led to a more aggradational or retrogradational stacking pattern (Figs 4 to 6). This is most obvious in the models with the highest sediment supply (22 km^3/kyr) as the deposits are thick enough to show these trends. The balance between the rate of sediment supply and the rate of base-level change determines whether the stacking pattern was more aggradational or retrogradational; the low sediment supply models (0.22 km^3/kyr) showed backstepping and even deposition of isolated terminal lobes (Fig. 6); the intermediate sediment supply models (2.2 km^3/kyr) also exhibited retrogradation until the hydrological parameters increase exponentially around −18 kyr and led to progradation; the high sediment supply models (22 km^3/kyr) showed progradation and aggradation as lake-level rise never outpaced sediment supply (Fig. 5).

Grain-size distribution, net to gross and sediment thickness

The plot of grain-size distribution (Fig. 7), NTG (Fig. 8) and sediment thickness (Fig. 9 for the scaled and Fig. S7 for the unscaled plot) displays the three-dimensional data as a pseudo downstream cross-section. Each point along the *x*-axis is the mean of all data points with that Euclidian distance from the apex. Missing plots or mean and mode values, and blanked out areas of plots, indicate that for those distances from the apex, the 50% coverage rule was not met. 'Net' in the NTG plot includes coarse to medium sands, fine to very fine sands, and silts, whereas 'Gross' encompasses all grain sizes.

In general, the grain-size distribution, NTG and sediment thickness were more sensitive to sediment supply rate change than to lake-level

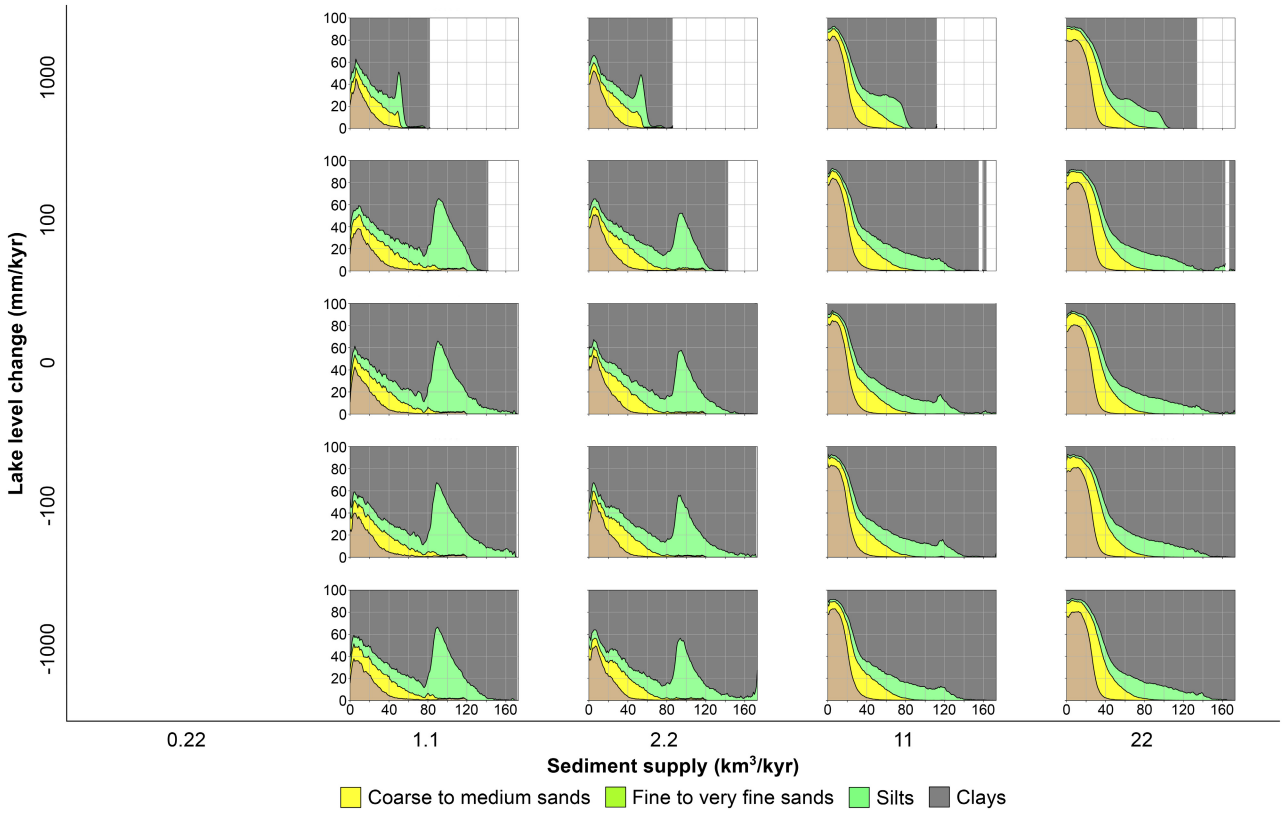

Fig. 7. Sediment supply – lake level change sensitivity models showing stacked grain-size distribution as pseudo downstream cross-section using a Euclidian distance from the apex. The *x*-axis depicts distance from the apex in kilometres and the *y*-axis total sediment thickness in metres. Missing plots or parts of plots indicate that less than half of the nodes with the same distance from the apex were filled and thus data analysis was not performed for these nodes.

change. The coarse to medium sand percentage (Fig. 7), mean NTG (Fig. 8) and mean sediment thickness (Fig. 9) increased with rate of sediment supply. Net to gross variability decreased with increasing sediment supply rate (Fig. 8). The higher the sediment supply rate, the lower the clay percentage in the proximal zones (Fig. 7). Bypass of coarser sediments to the distal zones occurred in low to mid sediment supply models (0.22 to 2.2 km^3/kyr). Additionally, with increasing sediment supply rate, NTG increased in the proximal zones and decreased in distal zones. The NTG distribution in the low to mid sediment supply models (0.22 to 2.2 km^3/kyr) was bimodal with NTG maxima in the proximal and distal zones (Fig. 8). The distal NTG peak occurred in thin deposits (Fig. 9) and contained mainly silts (Fig. 7). The distal peaks decreased in magnitude with increasing sediment supply rate and were not significant in the second highest and highest sediment supply models (11 km^3/kyr and 22 km^3/kyr). For the lowest sediment supply models (0.22 km^3/kyr), no sediments were deposited in the first 10 km downstream from the apex for the models with the highest lake-level rise (1000 mm/kyr) and for the first 16 km downstream from the apex for models with the other lake-level change scenarios (Fig. 9).

The higher the rate of lake-level rise, the closer to the apex the furthest downstream deposition occurred (Fig. 9). This was also the case for net grain sizes with silt constituting the main grain size in the distal zone (Fig. 7). For the lowest to medium sediment supply models (0.22 to 2.2 km^3/kyr), the models with lake-level rise (1000 mm/kyr and 100 mm/kyr) had the peak of coarse to medium sand deposition further downstream than the models with lake-level drop and static lake level (−1000 to 0 mm/kyr). The distal silt peak in these sediment supply models decreased in size with increasing

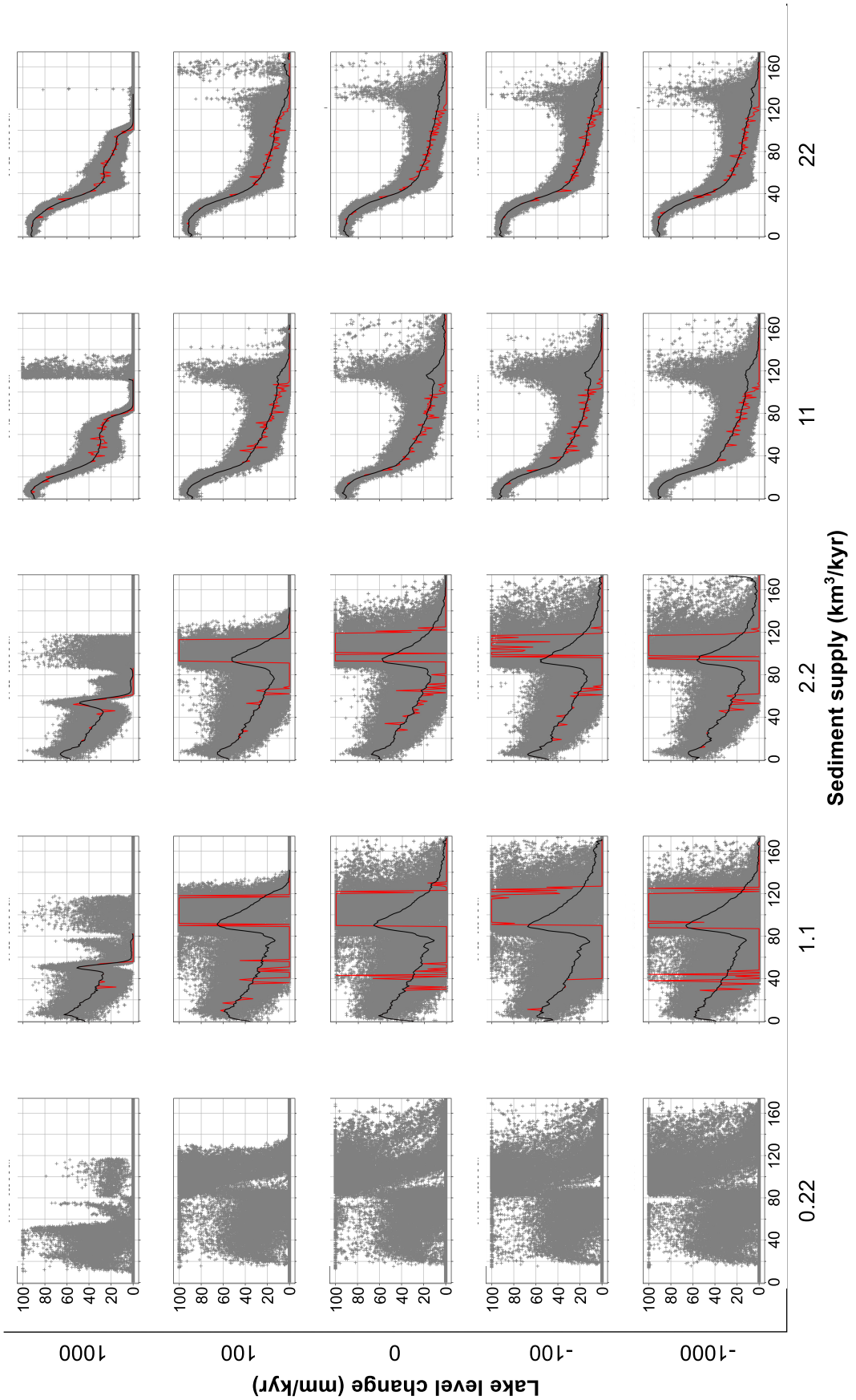

Fig. 8. Sediment supply – lake level change sensitivity models showing net to gross as pseudo downstream cross-section using a Euclidian distance from the apex. The *x*-axis depicts distance from apex in kilometres and the *y*-axis met to gross in percent. Each data point is shown as a grey cross, the mode as red line, and mean as black line. Missing mean and mode graphs indicate that less than half of the nodes with the same distance from the apex were filled and thus data analysis was not performed for these nodes.

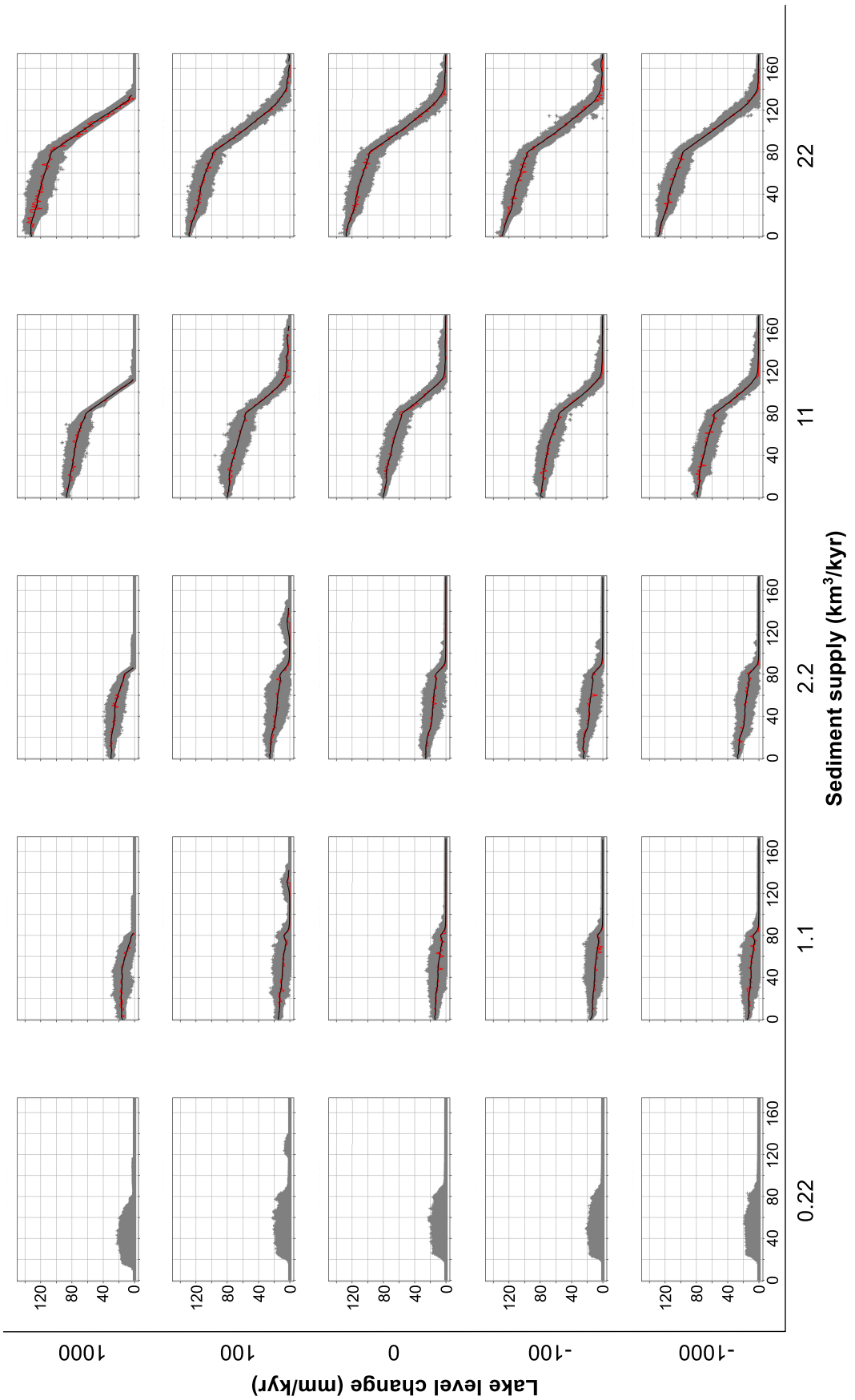

Fig. 9. Sediment supply – lake level change sensitivity models showing sediment thickness as pseudo downstream cross-section using a Euclidian distance from the apex. The *x*-axis depicts distance from apex in kilometres and the *y*-axis total sediment thickness in metres. The plots have a scaled *y*-axis. Each data point is shown as a grey cross, the mode as red line, and mean as black line. Missing mean and mode graphs indicate that less than half of the nodes with the same distance from the apex were filled and thus data analysis was not performed for these nodes.

lake level and was similar for the static and lake-level fall models. The peak of silt deposition was located at the break of slope in the initial surface from the steeper underlying DFS deposits and the shallower lacustrine zone (Fig. 1).

Sandbody thickness, number of sandbodies and amalgamation ratio

Sandbody thickness was defined as composite accumulation of a single or multiple channel, and splay elements that are amalgamated together into a multilateral and multi-storey body. The sandbody thickness (Fig. 10 for the scaled; Fig. S8 for the unscaled plot), number of sandbodies (Fig. 11 for the scaled; Fig. S9 for the unscaled plot) and amalgamation ratio (Fig. 12) plots are configured the same as the grain-size distribution, NTG and sediment thickness plots (Figs 7 to 9). As with the other parameters, sandbody thickness, number of sandbodies and amalgamation ratio, were more sensitive to sediment supply rate change than to lake-level change. In general, sandbody thickness increases exponentially with sediment supply rate (Fig. 10). The higher the sediment supply rate, the more numerous the sandbodies (Fig. 11) and the higher the mean amalgamation ratio (Fig. 12). Additionally, the higher the sediment supply rate, the higher the sandbody thickness variability. Lake-level rise created thicker sandbodies than lake-level fall (Fig. 10). The general downstream trend for the number of sandbodies also changed from decreasing linearly (1.1 km^3/kyr and 2.2 km^3/kyr), to a minimum around 10 km and a maximum around 30 km from the apex (11 km^3/kyr) to a minimum around 10 km and a maximum around 40 km from the apex (22 km^3/kyr). For the models in the highest two sediment supply rates (11 km^3/kyr and 22 km^3/kyr) the mean number of sandbodies followed a bimodal distribution with peaks at 30 km and 60 km downstream of the apex and 40 and 60 km downstream of the apex, respectively (Fig. 11). For the amalgamation ratio, the higher the sediment supply rate, the lower the variability and the higher the peak in the proximal zone and the smaller the peak in the distal zone. Only in the highest two sediment supply rates (11 km^3/kyr and 22 km^3/kyr), did the mean amalgamation ratio indicate nearly full connectivity in the proximal zone. Lastly, the amalgamation ratio variability in the distal zone decreased with increasing lake-level rise and stayed similar for both static and dropping lake level models (Fig. 12).

DISCUSSION

Sensitivity of a distributive fluvial system to changes in sediment supply and base-level

To explore the full potential of this sensitivity analysis, the parameters can be generalized (Fig. 13). The sediment supply can be simplified in this context as undersupplied (0.22 km^3/kyr), intermediate-supplied (1.1 km^3/kyr and 2.2 km^3/kyr) and oversupplied (11 km^3/kyr and 22 km^3/kyr). Lake-level change can be simplified as rising or falling base-level. This broadens the sensitivity analysis to other distributive fluvial system (DFS) termination types as described in Hartley *et al.* (2010) such as axial fluvial systems and coasts.

This study shows that DFS are more sensitive to sediment supply than to local base-level. When describing DFS sedimentology, Nichols & Fisher (2007) and Owen *et al.* (2015) divided DFS into three zones: proximal, medial and distal with decreasing average grain size. This description is based on the Huesca and Luna DFS in the Ebro Basin, northern Spain, the Devonian Munster Basin, southern Ireland, and the Salt Wash DFS of the Morrison Formation, south-western USA. Such zonation only matches the oversupplied models in this sensitivity analysis. The undersupplied models have no deposition in the proximal region due to erosion and sediment bypass, but have a medial region as described by Nichols & Fisher (2007) and Owen *et al.* (2015). The models with intermediate supply show deposition in the proximal and medial regions as described only for the medial zone in Nichols & Fisher (2007) and Owen *et al.* (2015). The distal zones of all sensitivity analysis models are as described in Nichols & Fisher (2007) and Owen *et al.* (2015) but the grain-size distribution within this zone is dependent on the local base-level (Fig. 13). When sediments reach local base-level, deposition is focussed at the interface between depositional surface and the base-level. This is especially true for silts. Sands can also accumulate at local base-level but only in the undersupplied models where sand bypass is common (Fig. 13). As only the models with base-level rise result in elevation of base-level above the initial depositional surface, the concentration of sands and silts occurs at

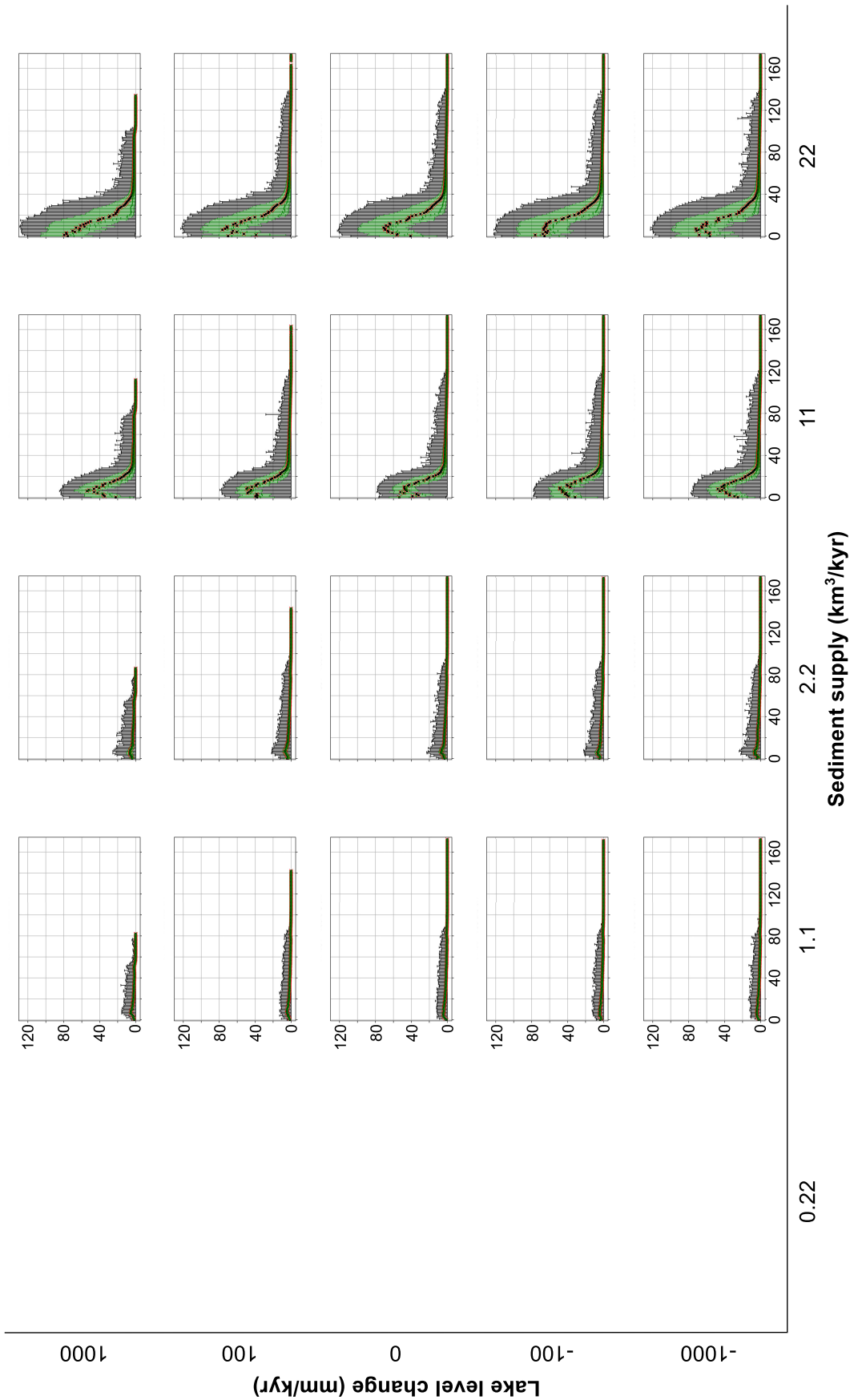

Fig. 10. Sediment supply – lake level change sensitivity models showing sandbody thickness as pseudo downstream cross-section using a Euclidian distance from the apex. The *x*-axis depicts distance from apex in kilometres and the *y*-axis sandbody thickness in metres. The plots have a scaled *y*-axis. The mode is shown as red crosses, the min–mean–max as black bars with the mean as a circle, and P90–P50–P10 as green bars with the P50 as cross. Missing plots or parts of plots indicate that less than half of the nodes with the same distance from the apex were filled and thus data analysis was not performed for these nodes.

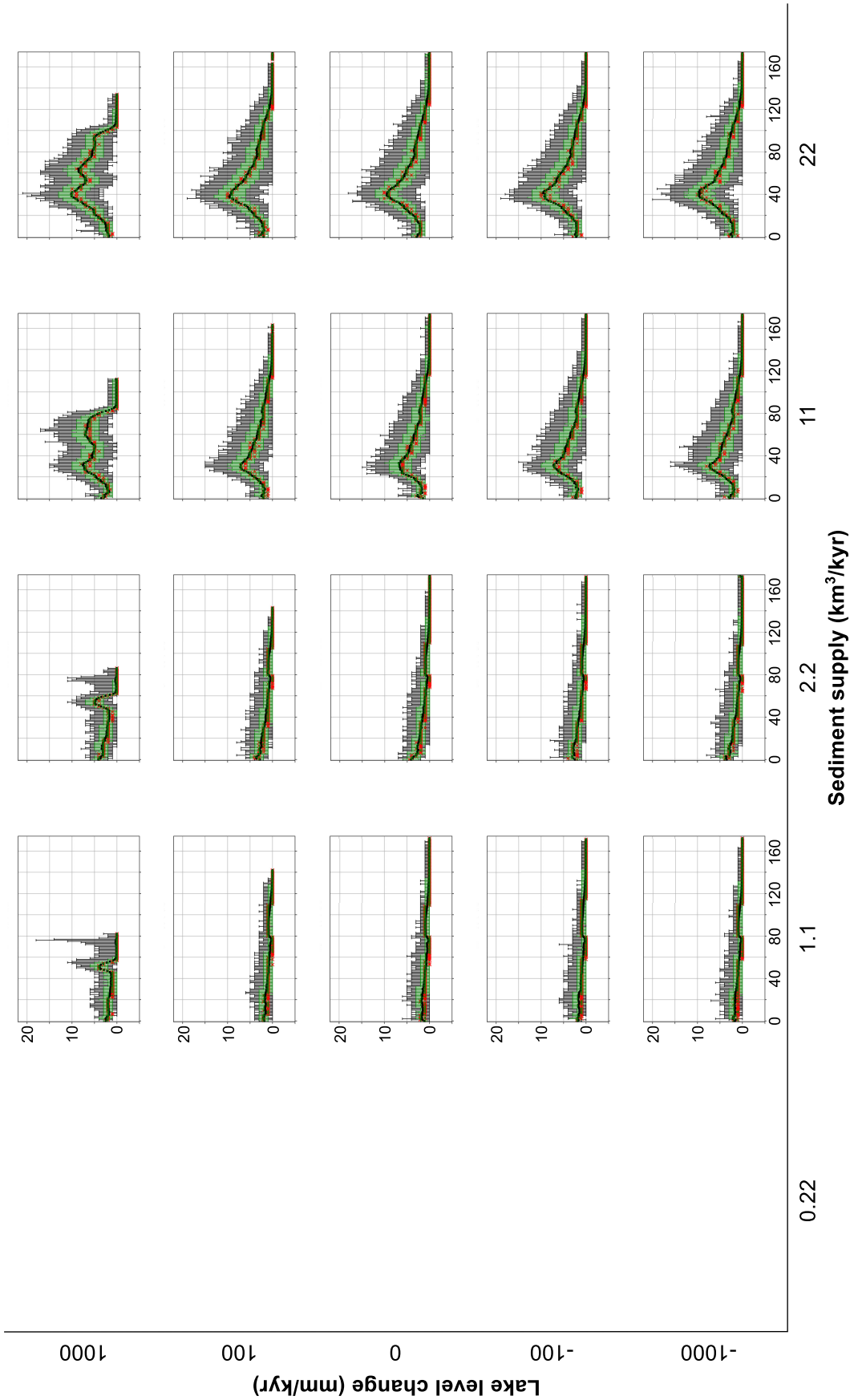

Fig. 11. Sediment supply – lake level change sensitivity models showing number of sandbodies as pseudo downstream cross-section using a Euclidian distance from the apex. The *x*-axis depicts distance from apex in kilometres and the *y*-axis number of sandbodies. The plots have a scaled *y*-axis. The mode is shown as red crosses, the min–mean–max as black bars with the mean as a circle, and P90–P50–P10 as green bars with the P50 as cross. Missing plots or parts of plots indicate that less than half of the nodes with the same distance from the apex were filled and data analysis was not performed for these nodes.

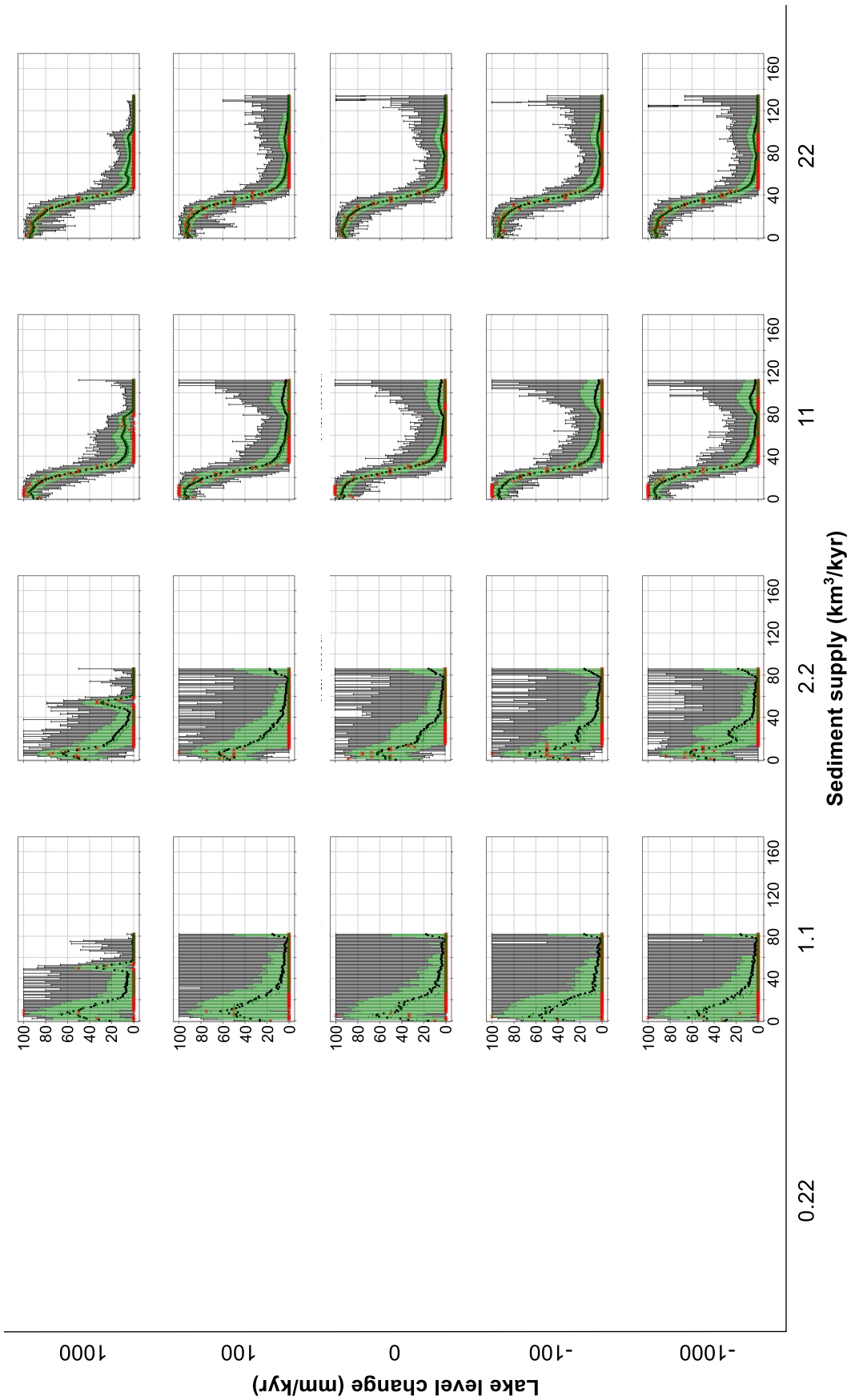

Fig. 12. Sediment supply – lake level change sensitivity models showing amalgamation ratio as pseudo downstream cross-section using a Euclidian distance from the apex. The *x*-axis depicts distance from apex in kilometres and the *y*-axis amalgamation ratio in percent. The mode is shown as red crosses, the min–mean–max as black bars with the mean as a circle, and P90–P50–P10 as green bars with the P50 as cross. Missing plots or parts of plots indicate that less than half of the nodes with the same distance from the apex were filled and data analysis was not performed for these nodes.

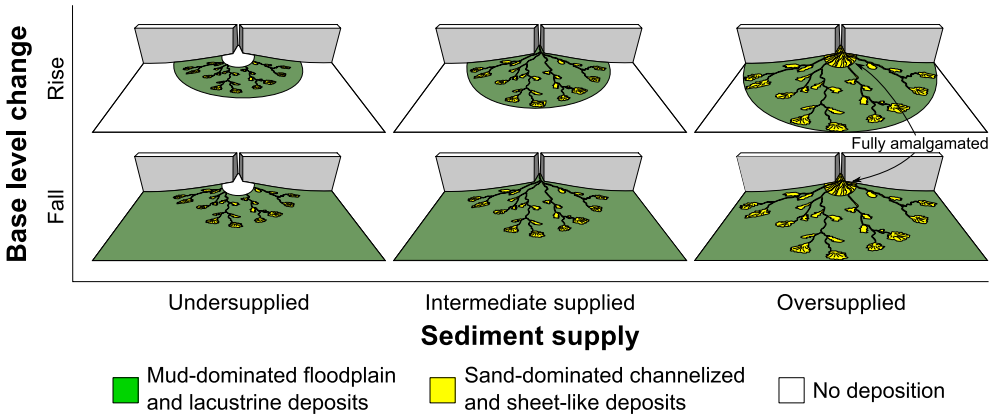

Fig. 13. Generalized sediment supply – lake level change sensitivity models showing the distribution of deposits. Only oversupplied models show the proximal, medial and distal zonation as described by Nichols & Fisher (2007) and Owen *et al.* (2015). The intermediate-supplied models do not have a fully amalgamated proximal zone while the undersupplied models have no deposition in the proximal area.

the lake shore (Fig. 13). Base-level rise also leads to deposition closer to the apex resulting in greater aggradation rates in the proximal zone and thicker sandbodies. In undersupplied and intermediate-supplied base-level rise models, the base-level rise outpaces sedimentation and results in retrogradation (Fig. 13). Undersupplied models experience retrogradation during the entire model duration whereas models with intermediate sediment supply only experience retrogradation until the hydrological parameters increase sufficiently to lead to progradation. Retrogradation produces isolated terminal fans that contain sands and silts (Fig. 13).

Models that simulate low rates of sediment supply have erosion in the proximal region and sediment bypass (even of coarse to medium sand and fine to very fine sand, to the distal region of the model), as they remain in the stabilization phase of DFS deposition during the entire model duration (Fig. 13). During the stabilization phase, the sediment supply generates a stable depositional surface, based on the grain-size distribution and depositional angles of each grain size, which is slightly different to the topography of the initial surface. The topography of the initial surface is also a depositional surface but generated by a different grain-size distribution and depositional angles. This stabilization phase is well-described in the stratigraphic model based on the Huesca DFS (Snieder *et al.*, 2021), which is also the base-case model for this sensitivity analysis. To shorten the stabilization phase in the sensitivity analysis models, the depositional surface of the Huesca DFS model after the stabilization phase was used. All sensitivity analysis models undergo an initial stabilization phase. In undersupplied models, insufficient sediment flowed into the model to stabilize during the model duration, but these models would eventually stabilize through higher sediment supply and/or longer model duration. This depositional behaviour is induced by the model setup but reproduces distributive fluvial systems that experienced an abrupt change in the hydrology and sediment distribution of the inflow into the system at the apex.

Characterization of accommodation and preservation in a distributive fluvial system

Holbrook *et al.* (2006) developed the concept of buffers and buttresses to define fluvial preservation space. This space is confined between upper and lower profiles called ‘buffers’. The upper buffer is defined as the profile of highest possible aggradation and the lower buffer is defined as the profile of maximum possible incision. These buffers are anchored downstream by a physical barrier such as a lake shore that is called a ‘buttress’.

In the models, the upper buffer is created by the combined maximum depositional gradient of sediment present in the DFS. The maximum depositional gradient increases with increasing grain size. As the grain-size distribution in DFS becomes more fine-grained from the apex to the toe of the system (Fig. 7), the maximum depositional gradient decreases. The maximum depositional gradient is set in the modelling parameters for each grain size and is identical for all models. The lower

buffer in the models is the graded profile anchored downstream at the buttress. The buttress is the lake shore as it is the intersection between the DFS and the base-level. In map view, the fluvial preservation space (Holbrook *et al.*, 2006) is shaped like the DFS, which in case of the sensitivity analysis models is semi-circular (Fig. 4). In addition to the downstream component of the fluvial preservation space described by Holbrook *et al.* (2006), the DFS models also include the upstream component.

The DFS modelling has shown that the lower and upper buffers converge at the lake shore (downstream anchor point) and at the DFS apex (upstream anchor point). As opposed to the conceptual models proposed by Holbrook *et al.* (2006), these two anchor points can move both vertically and laterally with time. The lake shore can move upstream during transgression or downstream during regression. The lake shore transgresses when the rate of lake-level rise outpaces the rate of sediment supply, as is the case in the 'undersupplied' models that incorporate an episode of lake-level rise. The lake shore regresses when sediment supply outpaces lake-level rise such as in the 'oversupplied' models. The lake shore can remain in the same plan-view position if sediment supply and lake-level rise are equal, and aggradation occurs. The apex moves upstream when aggradation occurs in the proximal zone such as in the 'intermediate-supplied' and 'oversupplied' models. Downstream movement occurs when base-level lowering, subsidence, and/or sediment supply changes lead to incision and a downstream shift in the DFS including the apex. Holbrook & Bhattacharya (2012) coined this incision 'buffer valleys' and it can be observed in the modern Taquari DFS, western Brazil, where the palaeo-DFS is incised for the first 100 km downstream of the palaeo-apex before reaching the present-day apex and the start of the present-day fan (Assine & Soares, 2004; Assine, 2005; Buehler *et al.*, 2011; Makaske *et al.*, 2012). The non-deposition in the proximal region of the undersupplied models is not due to a downstream movement of the apex but due to the adjustment of the modelled sediment erosion, transport and deposition to the initial surface.

The lower buffer is anchored to the buttress so the models with a falling base-level also have a lowering surface of maximum possible incision. Incision starts at the buttress and moves upstream (Holbrook *et al.*, 2006). Such incision is not observed in the base-level fall models. Incision would occur in the distal part of the model, which is mostly uncovered by sediment. Thus, the initial surface would be incised into underlying strata. The initial surface hardness is set to the erodibility of uncompacted sediment, which means that erosion will occur if the velocity of any fluvial flow reaching this region is high enough to be erosive (Hjulström, 1935; Sundborg, 1956). Even in the oversupplied static base-level models, little to no sediment was transported to the most distal parts of the model (Figs 4 and 9) as the fluvial transport capacity was insufficient. If flow velocity was not sufficient to transport sediment, it would not have any erosive power for incision (Hjulström, 1935; Sundborg, 1956). Holbrook *et al.* (2006) described the lower buffer as a surface of maximum possible incision, but this possibility is only realized if the fluvial flow has sufficient erosive power.

The DFS modelling has also shown that the space described by Holbrook *et al.* (2006) as fluvial preservation space, is the fluvial accommodation available in the DFS at each point in time for a given apex and lake shore location and a given underlying surface and grain-size distribution. If the sediment supply is greater than the fluvial accommodation at that point in time, then the apex location will move up the feeder valley and the lake shore location will regress as excess sediment is deposited in a lacustrine delta. This can be calculated for the sensitivity analysis models. To simplify the process, the calculations are only for the models with static base-level (0 mm/kyr) and assume an even distribution of sediment over the DFS in map view. The two models chosen are the second to lowest sediment supply model (1.1 km^3/kyr) and the highest sediment supply model (22 km^3/kyr). The lowest sediment supply model was not chosen since less than half of the DFS surface is covered, it does not satisfy the above-mentioned assumption of deposition over the entire DFS surface. The proxy for sediment supply is the mean gradient of the final depositional surface and the proxy for fluvial accommodation is the maximum depositional gradient based on the grain-size distribution of the DFS deposit after the 100 kyr of modelling. For the second to lowest sediment supply model (1.1 km^3/kyr), the sediment supply proxy is a gradient of 0.0015 and the fluvial accommodation proxy is a gradient of 0.0022. This means that the given fluvial accommodation for the 100 kyr of model duration was only 68% filled. For the highest sediment supply model (22 km^3/kyr), the sediment supply proxy is a gradient of 0.0023 and the fluvial accommodation proxy is a gradient of 0.0023 as well. This means that the sediment supply has overfilled the initial fluvial

accommodation and further accommodation is created by upstream migration of the apex and downstream migration of the lake shore. This clearly shows that sediment supply and fluvial accommodation are interdependent governing parameters. It also shows that grain-size distribution of the sediment flowing into the DFS, and the underlying surface topography are crucial to linking the governing parameters.

Besides the governing parameters, elapsed time also plays a key role in understanding DFS accommodation and preservation. The models encompass 100 kyr, which means that extreme changes in governing parameters, such as the sediment supply spike around −18 kyr (Fig. 2) and rapidly rising base-level (highest lake-level rise models), require more time for the DFS to adapt than was modelled.

It should be noted that each sensitivity analysis is specific to the limitations of the sensitivity parameter range. It is for this reason that such large ranges were chosen for this analysis, and for the other modelling parameters, mainly model duration, initial surface topography, sediment classes and maximum depositional angles. This highlights the complex interdependencies between the governing parameters acting on DFS.

CONCLUSIONS

This sensitivity analysis of distributive fluvial system (DFS) architecture to sediment supply and base-level change revealed that DFS facies distribution is significantly more sensitive to sediment supply than to base-level change. With increasing sediment supply, average grain size, aggradation rates and sandbody connectivity increase for a given distance from the fan apex. Base-level rise mostly influences DFS through sediment retention and concentration of silts in the vicinity of the lake shoreline. If base-level rise outpaces sedimentation, then coarser-grained deposits can become encased by deposits from the mud-dominated distal zone. Base-level rise also leads to higher aggradation rates and thicker sandbodies in the proximal zones.

Undersupplied DFS, defined as systems with sediment supply rates of at least one order of magnitude lower than the previous DFS they overlay, show no deposition in the proximal region, channelized sandy deposits within a fine-grained floodplain environment in the medial region, and a mud-dominated distal region. Distributive fluvial systems with intermediate sediment supply, defined as systems with sediments supply rates within plus or minus one order of magnitude than the previous DFS they overlay, have the same facies distribution as undersupplied DFS but medial type deposits are also deposited in the proximal region. Oversupplied DFS, defined as systems with sediment supply rates of at least one order of magnitude higher than the previous DFS they overlay, have a facies distribution and sandbody connectivity as described in Nichols & Fisher (2007) and Owen *et al.* (2015) with a fully amalgamated proximal zone of channelized deposits, which form a single sandbody, channelized deposits within a floodplain environment in the medial zone, and the same distal zone as the undersupplied and intermediate-supplied DFS. The results of all sensitivity models predict an initial stabilization phase. During this phase a new depositional slope, as a function of the model parameters, is formed on top of the initial surface. The 'undersupplied' models never evolve beyond this phase, which is why non-deposition occurs in the proximal region.

The sensitivity analysis also indicated that the concept of buffers and buttresses (Holbrook *et al.*, 2006) is probably applicable to DFS. The buttress is the lake shore as it is the intersection between the DFS and the base-level. The upper buffer is the product of the combined maximum depositional gradient of sediment present in the DFS. As the maximum depositional gradient decreases with decreasing grain size and the grain-size distribution also decreases downstream of the DFS' apex, the slope of the upper buffer decreases downstream of the apex of the DFS. The lower buffer in the models is the graded profile anchored downstream at the buttress. The buffers not only converge downstream towards the buttress but also upstream at the DFS apex. These anchor points are shown to be mobile in upstream, downstream and/or vertical directions. The movement of these anchor points allows a quantification of accommodation and preservation. Upstream movement of the upper anchor point (DFS apex) indicates aggradation in the proximal zone. Downstream movement of the apex and incision upstream of the apex indicates base-level lowering, subsidence and/or sediment supply changes. Upstream movement of the buttress indicates transgression and downstream movement indicates regression. If sediment supply and lake-level rise are in equilibrium, then the buttress remains in the same plan-view position. Incision in the distal region was not observed in the model results

with base-level fall as the flow reaching these regions did not have enough erosive power.

This sensitivity analysis highlights the interdependency of governing parameters acting on the DFS. Besides the two main parameters of sediment supply and lake-level change investigated in this project, other governing parameters such as the topography of the initial surface, the grain-size distribution of the sediments introduced at the source, and the maximum depositional gradients for each sediment class have a strong impact on the stratigraphic architecture of DFS. Lastly, elapsed time is crucial to understand the processes that govern the sedimentary and stratigraphic evolution of DFS. The results of this sensitivity analysis must be considered in the context of the modelled time frame. The same applies to characterizing DFS accommodation and preservation. These are time-dependent variables and should be treated as such.

ACKNOWLEDGEMENTS

This study was part of a doctoral project financed through a studentship by the United Kingdom Research and Innovation Centre for Doctoral Training in Oil and Gas, which was institutionally funded by the University of Aberdeen, United Kingdom. An academic licence of the stratigraphic forward modelling software SedsimX was provided by StrataMod Pty. Limited, Australia. The authors want to thank John Wood, Prabhat Hegde and Ramy Abdallah for their help with coding of the model processing scripts. The authors would also like to thank reviewer Nigel Mountney for constructive comments which helped to improve this manuscript.

DATA AVAILABILITY STATEMENT

The data that support the findings of this study are openly available on request to the first author due to the large file size.

REFERENCES

Assine, M.L. (2005) River avulsions on the Taquari megafan, Pantanal wetland, Brazil. *Geomorphology*, **70**, 357–371.

Assine, M.L. and **Soares, P.C.** (2004) Quaternary of the Pantanal, west-central Brazil. *Quat. Int.*, **114**, 23–34.

Best, J.I.M. and **Fielding, C.R.** (2019) Describing fluvial systems: linking processes to deposits and stratigraphy. *Geol. Soc. Spec. Pub.*, **488**, 151–166.

Bridge, J.S. (2003) Bedset and laminaset. In: *Encyclopedia of Sediments and Sedimentary Rocks* (Eds Middleton, G.V., Church, M.J., Coniglio, M., Hardie, L.A. and Longstaffe, F.J.), pp. 59–61. Springer, Dordrecht.

Buehler, H.A., **Weissmann, G.S.**, **Scuderi, L.A.** and **Hartley, A.J.** (2011) Spatial and temporal evolution of an avulsion on the Taquari river distributive fluvial system from satellite image analysis. *J. Sediment. Res.*, **81**, 630–640.

Chen, C. and **Hiscott, R.N.** (1999) Statistical analysis of facies clustering in submarine-fan turbidite successions. *J. Sediment. Res.*, **69**, 505–517.

Colombera, L., **Mountney, N.P.** and **McCaffrey, W.D.** (2015) A meta-study of relationships between fluvial channel-body stacking pattern and aggradation rate: implications for sequence stratigraphy. *Geology*, **43**, 283–286.

Coronel, M.D., **Isla, M.F.**, **Veiga, G.D.**, **Mountney, N.P.** and **Colombera, L.** (2020) Anatomy and facies distribution of terminal lobes in ephemeral fluvial successions: Jurassic Tordillo Formation, Neuquén Basin, Argentina. *Sedimentology*, **67**, 2596–2624.

Couchoud, I., **Genty, D.**, **Hoffmann, D.**, **Drysdale, R.** and **Blamart, D.** (2009) Millennial-scale climate variability during the Last Interglacial recorded in a speleothem from south-western France. *Quatern. Sci. Rev.*, **28**, 3263–3274.

Felletti, F. (2004) Spatial variability of Hurst statistics in the Castagnola Formation, Tertiary Piedmont Basin, NW Italy: discrimination of sub-environments in a confined turbidite system. *Geol. Soc. Lond. Spec. Publ.*, **222**, 285–305.

Felletti, F. and **Bersezio, R.** (2010) Validation of Hurst statistics: a predictive tool to discriminate turbiditic sub-environments in a confined basin. *Petrol. Geosci.*, **16**, 401–412.

Griffiths, C.M., **Dyt, C.**, **Paraschivoiu, E.** and **Liu, K.** (2001) Sedsim in hydrocarbon exploration. In: *Geologic Modeling and Simulation* (Eds Merriam, D. and Davis, J.C.), pp. 71–97. Kluwer Academic, New York, NY.

Groten, J.T., **Ellison, C.A.** and **Hendrickson, J.S.** (2016) Suspended-Sediment Concentrations, Bedload, Particle Sizes, Surrogate Measurements, and Annual Sediment Loads for Selected Sites in the Lower Minnesota River Basin, Water Years 2011 through 2016. In: *U.S. Geological Survey Scientific Investigations Report 2016–5174*. U.S. Geological Survey, Reston, VA.

Hartley, A.J., **Weissmann, G.S.**, **Nichols, G.J.** and **Warwick, G.L.** (2010) Large distributive fluvial systems: characteristics, distribution, and controls on development. *J. Sediment. Res.*, **80**, 167–183.

Hjulström, F. (1935) *Studies of the Morphological Activity of Rivers as Illustrated by the River Fyris*. Inaugural dissertation. Almqvist & Wiksells, Uppsala, Sweden.

Holbrook, J.M. and **Bhattacharya, J.P.** (2012) Reappraisal of the sequence boundary in time and space: case and considerations for an SU (subaerial unconformity) that is not a sediment bypass surface, a time barrier, or an unconformity. *Earth-Sci. Rev.*, **113**, 271–302.

Holbrook, J., **Scott, R.W.** and **Oboh-Ikuenobe, F.E.** (2006) Base-level buffers and buttresses: A model for upstream versus downstream control on fluvial geometry and architecture within sequences. *J. Sediment. Res.*, **76**, 162–174.

Huang, X., **Griffiths, C.M.** and **Liu, J.** (2016) Recent development in stratigraphic forward modelling and its application in petroleum exploration. *Aust. J. Earth Sci.*, **62**, 903–919.

Hurst, H.E. (1951) Long-term storage capacity of reservoirs. *Trans. Am. Soc. Civil Eng.*, **116**, 770–799.

Imbrie, J., **Boyle, E.A.**, **Clemens, S.C.**, **Duffy, A.**, **Howard, W.R.**, **Kukla, G.**, **Kutzbach, J.**, **Martinson, D.G.**, **McIntyre, A.**, **Mix, A.C.**, **Molfino, B.**, **Morley, J.J.**, **Peterson, L.C.**,

Pisias, N.G., **Prell, W.L.**, **Raymo, M.E.**, **Shackleton, N.J.** and **Toggweiler, J.R.** (1992) On the structure and origin of major glaciation cycles 1. Linear responses to milankovitch forcing. *Paleoceanography*, **7**, 701–738.

Laskar, J., **Robutel, P.**, **Joutel, F.**, **Gastineau, M.**, **Correia, A.C.M.** and **Levrard, B.** (2004) A long-term numerical solution for the insolation quantities of the Earth. *Astron. Astrophys.*, **428**, 261–285.

Lisiecki, L.E. and **Raymo, M.E.** (2005) A Pliocene-Pleistocene stack of 57 globally distributed benthic δ18O records. *Paleoceanography*, **20**, 1–17.

Makaske, B., **Maathuis, B.H.P.**, **Padovani, C.R.**, **Stolker, C.**, **Mosselman, E.** and **Jongman, R.H.G.** (2012) Upstream and downstream controls of recent avulsions on the Taquari megafan, Pantanal, south-western Brazil. *Earth Surf. Process. Landf.*, **37**, 1313–1326.

Mukhopadhyay, B., **Chakraborty, P.P.** and **Paul, S.** (2003) Facies clustering in turbidite successions: case study from Andaman Flysch Group, Andaman Islands, India. *Gondwana Res.*, **6**, 918–925.

Nichols, G.J. and **Fisher, J.A.** (2007) Processes, facies and architecture of fluvial distributary system deposits. *Sediment. Geol.*, **195**, 75–90.

Nyquist, H. (1928) Certain topics in telegraph transmission theory. *Trans. Am. Inst. Electr. Eng.*, **47**, 617–644.

Owen, A., **Nichols, G.J.**, **Hartley, A.J.**, **Weissmann, G.S.** and **Scuderi, L.A.** (2015) Quantification of a distributive fluvial system: the Salt Wash DFS of the Morrison Formation, SW U.S.A. *SEPM J. Sediment. Res.*, **85**, 544–561.

Ringrose, P. and **Bentley, M.** (2015) *Reservoir model design*, 1st edn. Springer Netherlands, Dordrecht, NL.

Shannon, C.E. (1949) Communication in the presence of noise. *Proc. IRE*, **37**, 10–21.

Snieder, S., **Griffiths, C.M.**, **Owen, A.**, **Hartley, A.J.** and **Howell, J.A.** (2021) Stratigraphic forward modelling of distributive fluvial systems based on the Huesca System, Ebro Basin, northern Spain. *Basin Res.*, **33**, 3137–3158.

Sundborg, Å. (1956) The river Klarälven: a study of fluvial processes. *Geogr. Ann.*, **38**, 238–316.

Tetzlaff, D.M. and **Harbaugh, J.W.** (1989) *Simulating Clastic Sedimentation*. Springer, New York, NY.

Weissmann, G.S., **Hartley, A.J.**, **Nichols, G.J.**, **Scuderi, L.A.**, **Olson, M.**, **Buehler, H.A.** and **Banteah, R.** (2010) Fluvial form in modern continental sedimentary basins: distributive fluvial systems. *Geology*, **38**, 39–42.

Weissmann, G.S., **Hartley, A.J.**, **Scuderi, L.A.**, **Nichols, G.J.**, **Owen, A.**, **Wright, S.**, **Felicia, A.L.**, **Holland, F.** and **Anaya, F.M.L.** (2015) Fluvial geomorphic elements in modern sedimentary basins and their potential preservation in the rock record: a review. *Geomorphology*, **250**, 187–219.

Zhang, L., **Wang, H.**, **Li, Y.** and **Pan, M.** (2017) Quantitative characterization of sandstone amalgamation and its impact on reservoir connectivity. *Petrol. Explor. Develop.*, **44**, 226–233.

Manuscript received 10 July 2022; revision accepted 1 May 2023

Supporting Information

Additional information may be found in the online version of this article:

Appendix S1. Detailed description of the source modulation including the link between discharge and flow velocity, and discharge and sediment supply based on the Minnesota River gauging station at Fort Snelling State Park, Minnesota, USA, as well as the climate proxy calculation for all sediment supply model. Additionally, unscaled sediment supply – lake level change sensitivity models showing sediment thickness, sandbody thickness and number of sandbodies.

